Time-domain induced polarization as a tool to image clogging in constructed wetlands

R. Garcia-Artigas[a, b], M. Himi[b], A. Revil[c], A. Urruela[b], R. Lovera[a, b], A. Sendrós, A[a, b]. Casas[a, b], and L. Rivero[a, b]

[a] Water Research Institute (IdRA). University of Barcelona, 08028 Barcelona, Spain.
[b] Mineralogy, Petrology and Applied Geology department. Faculty of Earth Sciences. University of Barcelona, 08028 Barcelona, Spain.
[c] Université Grenoble Alpes, USMB, CNRS, EDYTEM, 73000 Chambéry, France.

Email: r.garcia@ub.edu; himi@ub.edu; andre.revil@univ-smb.fr; aritz.urruela@ub.edu; rlovera@ub.edu; alex.sendros@ub.edu; albert.casas@ub.edu; lrivero@ub.edu

Corresponding Author: André Revil andre.revil@univ-smb.fr
Keywords: Obstruction, chargeability, constructed wetland, clogging.

Highlights:

(1) The time-domain induced polarization is used to image the clogging distribution in a constructed wetland. (2) A linear correlation between normalized chargeability and the amount of clogging is observed. (3) The effectiveness of the normalized chargeability as a proxy for the clogging presence is therefore demonstrated and applied in field conditions.

Intended for publication in Science of the Total Environment

Abstract. During the last decade, constructed (artificial) wetlands have flourished in Europe in order to treat sewage from small communities thanks to its low cost of operation and simplicity. That said, the clogging of the gravel filters is an issue that can affect their efficiency. The present work shows the results of the application of a geophysical method called time-domain induced polarization to non-intrusively image in 3D the clogging of the gravel filters in a quick and efficient way. Induced polarization characterizes the ability of a porous material to store reversibly electrical charges when submitted to an electrical field. The material property characterizing this ability is called normalized chargeability. We have developed a laboratory experiment to determine an empirical relationship between the normalized chargeability and the volumetric amount of clogging. Induced polarization measurements have been performed over a constructed wetlands to get a 3D reconstructed image (tomography) of the normalized chargeability. From this tomography and the previously defined relationship, we are able to image in 3D the amount of clogging. We can therefore identify the areas where this clogging is concentrated in the filter, an important task in order to take preventive measures to minimize this issue.

1. Introduction

During the last decade, constructed (artificial) wetlands have been developed for the treatment of waste water of small communities of less than ~2000 people (e.g., Puigagut et al., 2007) as well as for treating industrial wastewater, greywater, and stormwater runoff. Constructed wetlands are engineered systems that have been designed to take advantage of the same filtration processes that occur in natural wetlands (e.g. Vymazal, 2005; Puigagut et al. 2007; Vera et al. 2011). This filtration process involves the influence of wetland vegetation and the role of microbial assemblages. The idea is to apply this knowledge to assist waste water treatment in a more controlled environment. Constructed wetlands may be categorized following their design parameters: hydrology (open surface flow of water versus subsurface flow), type of macrophytes (emerged, submerged, free-floating or none), and flow paths (horizontal versus vertical) (see Vymazal, 2011).

Constructed wetlands act as a biofilter, filtering nutrients, organic matter, pathogens from the wastewater. It is therefore perhaps not surprising that the main problem affecting constructed wetlands is the development of clogging. Above a critical level; clogging can obstruct the porous filter in which water is flowing. Clogging include the role of inorganic and organic particles, the development of biofilms, plant biomass and accumulation of chemical precipitates (Pedescoll et al., 2011). Some approaches have been developed to minimize the development of clogging like the pretreatment of the influent in order to eliminate solids in suspension and favouring the removal of the macrophytes responsible for clogging (Pedescoll et al., 2011). There have been many attempts to limit or remedy to filter clogging. In this perspective, chemical treatments to oxidize the organic matter of the filter using hydrogen peroxide has appeared as a potential solution (Nivala and Rousseau, 2009), That said, engineers need to understand and if possible visualize flow paths and the occurrence of clogging in the subsurface. The traditional restoration procedure to a constructed wetland is to remove the clogged bed media and replace it with clean media or, if it is a gravel-based system, wash it and return it to the wetland bed. Both approaches are costly and may require sections of the facility to be taken offline for extended periods of time (Nivala and Rousseau, 2009).

Existing classical techniques to understand the flow paths include tracer tests (Marzo et al. 2018) and measurements of the hydraulic conductivity in a set of piezometers installed in the filter (Marzo et al. 2018 and Licciardello et al. 2019). In this perspective geophysical techniques such as the geo-radar (Tapias et al., 2013, Matos et al., 2019) and electrical resistivity tomography (Tapias et al., 2013, Marzo et al., 2018) can play a strong role in characterizing the filter. In order to be efficient in these approaches, non-intrusive techniques able to quantify clogging would be extremely useful. However, to our knowledge, no geophysical techniques provides a quantitative idea of the amount of clogging in the subsurface.

Induced polarization is a geophysical technique that can be used to image two key-properties of the subsurface, namely the electrical conductivity and the normalized chargeability. The former refers to the ability to porous media to conduct an electrical current while the second refers to the reversible accumulation of charge carriers (low frequency polarization) under the influence of a primary electrical field (Schlumberger, 1920). The grains and bacteria are coated by an electrical double layer, which is responsible for the polarization of the material. A recently developed model called the dynamic Stern layer concept (the Stern layer being the inner part of the double layer coating the surface of the grains and bacteria) seems to explain all induced polarization measurements to date made in the laboratory as well as in the field (see Rosen et al., 1993; Revil and Florsch, 2010; Revil, 2012, 2013a).

The motivation for our work is based on the following observatons and modelling effort. We know that the dynamic Stern layer model of induced polarization implies that the normalized chargeability is strongly controlled by both the Cation Exchange Capacity (CEC) of clay materials (Revil, 2012, 2013a) and the presence of bacteria (Revil et al., 2012; Zhang et al., 2014). Since clogging materials are expected to have a strong CEC and biolfilms are present, imaging the normalized chargeability distribution of constructed wetlands is the key to quantify the amount of clogging in the porous filter. We want to test this idea in this work. If we can non-intrusively image clogging, this also means that we can monitor its occurrence, both in space and time, and therefore anticipate complete clogging of the porous filter and reduce *ipso facto* the cost of maintenance of these system.

2. Materials and methods

An operational wetland located in Vedú (Spain) is used as a test site in the present study. This constructed wetland treats the urban wastewater from Verdú (population of 919 people in 2019) with a maximum designed flow rate of 400 m^3/d. This waste water treatment system includes a pre-treatment of the waste water consisting on three septic tanks in parallel to each other (Figure 1). The resulting effluent is distributed to four gravel-based horizontal subsurface flow constructed wetlands. After these constructed wetlands, the pore water goes through two maturation ponds and finally two additional small horizontal subsurface flow constructed wetlands (Figure 1). This site entered into operation in 2002. All the four gravel-based horizontal subsurface flow units have been affected by clogging problems. This issue was minimized by operating regularly some gravel cleaning or substitution, which had the drawback to increase the operational cost of the site.

2.1 Induced polarization

Induced polarization is a non-intrusive geophysical method investigating the ability of porous materials to store reversibly electric charges under the action of an external (primary) electrical field (Vinegar and Waxman, 1984 and Figure 2). Induced polarization measurements can be performed in time-domain (TDIP) or frequency domain (FDIP), but in the field TDIP measurements are preferred over FDIP because of their easiness to be carried out with most resistivity meters.

The TDIP conceptualization data is sketched in Figure 3. A box current is injected into the ground using two current electrodes (A and B) over a period T (typically T = 1 s) The resulting electrical potential distribution is recorded between two potential electrodes (M and N). In this study we use stainless steel electrodes. When the primary current is shut down, the secondary current decays over time (Figure 3, Schlumberger, 1920). This decay expresses the fact that the stored electrical charges comes back to their statistical equilibrium position by electro-diffusion (e.g., Revil, 2013b). In order to image the chargeability, the voltage curve is sampled over a series of windows. Then, the polarization data are formed by partial (apparent) chargeabilities (dimensionless but often expressed in mV/V). These partial chargeabilities M_i are obtained by integrating the secondary voltage decay between times t_i and t_{i+1}.

$$M_i = \frac{1}{\psi_0(t_{i+1}-t_i)}\int_{t_i}^{t_{i+1}} \psi(t)\mathrm{d}t. \quad (1)$$

In this equation, ψ_0 denote the potential difference between the voltage electrodes M and N just before the shutdown of the primary current, $\psi(t)$ denote the secondary voltage decay curve associated with ground polarization, t_i+1 - t_i indicates the duration of the window W_i. During the acquisition, it is recommended to separate the cables for the current injection (containing all the bipoles AB) and the cable used for the voltage measurements (containing all the voltage electrodes MN, see Dahlin and Leroux, 2012). This is done to minimize electromagnetics capacitive and inductive couplings between the wires and to avoid the potential electrodes (M and N) polarization, preventing to use them as current electrodes (A and B).

In order to interpret induced polarization tomograms, we need to describe a fundamental model developed in the past decade and called the dynamic Stern layer model (e.g., Rosen et al., 1993; Revil, 2013b). This model implies that most of the observed polarization in a metal-free porous materials is due to the polarization of the Stern layer coating the surface of the grains. This Stern layer forms the inner part of the electrical double layer coating the grains. Considering that an external harmonic electric field $\mathbf{E} = \mathbf{E}_0 \exp(+i\omega t)$, $\mathbf{E}_0$ (V m^{-1}) denotes the amplitude, ω denotes the pulsation frequency (in rad s^{-1}), and t (in s) is time applied to a porous material (primary field), the complex conductivity of the porous rock can be written as (Revil et al., 2017b)

$$\sigma^*(\omega) = \sigma_\infty - M_n \int_0^\infty \frac{h(\tau)}{1+(i\omega\tau)^{1/2}} d\tau \,. \quad (2)$$

The quantity ω denotes the pulsation frequency (expressed in rad s $^{-1}$), $h(\tau)$ designates a probability density for distribution of the relaxation times associated with charges accumulations at grain scales. In equation (1), M_n signifies the normalized chargeability (expressed in S m^{-1}) (Seigel, 1959; Revil et al., 2017) as

$$M \equiv \frac{\sigma_\infty - \sigma_0}{\sigma_\infty}, \tag{3}$$

$$M_n \equiv \sigma_\infty - \sigma_0, \tag{4}$$

where σ_∞ and σ_0 (both in S m^{-1}) denote the instantaneous and DC (Direct Current) conductivity of the porous material, respectively. The quantity σ_∞ corresponds to the conductivity just after the application of the external (primary) electrical field. In this situation, all the charge carriers are mobile (Revil et al., 2017a). The quantity σ_0 (S m^{-1}) defined the conductivity of the material for a long application of the electrical field corresponding to steady-state condition. (Revil et al., 2017a). The DC conductivity is necessarily smaller than the instantaneous conductivity since the charges responsible for the polarization are not available anymore for the conduction process. Extending Archie's law (Archie, 1942) to include surface conductivity effects, Revil (2013b) obtained the following expressions of the high and low-frequency conductivities,

$$\sigma_\infty = \theta^2 \sigma_w + \theta \rho_g B \,\mathrm{CEC}, \tag{5}$$

$$\sigma_0 = \theta^2 \sigma_w + \theta \rho_g (B - \lambda) \mathrm{CEC}. \tag{6}$$

Respectively, and therefore, the normalized chargeability is given by

$$M_n = \theta \rho_g \lambda \,\mathrm{CEC}. \tag{7}$$

In these equations, θ denotes the volumetric water content (equal to the porosity at saturation), σ_w (in S m^{-1}) is the pore water conductivity, ρ_g designates the grain density (in kg m^{-3}, usually ρ_g = 2650 kg m^{-3}), and CEC (C kg^{-1} where C stands for Coulomb) signifies the cation exchange capacity of the material. This CEC corresponds to the density of exchangeable surface sites on the surface of the mineral grains. It is typically measured using titration experiments in which the surface of the grains is exchanged with a cation having a high affinity for the sites populating the mineral surface. It is often expressed in meq/100 g with 1 meq/100 g = 963.20 C kg^{-1}. In equations (3) and (4), B (in m^{2}s^{-1}V^{-1}) denotes the apparent mobility of the counterions for surface conduction. By surface conduction, we mean the conductivity associated with conduction in the electrical double layer coating the surface of the grains. The quantity λ (in m^{2}s^{-1}V^{-1}) symbolizes the apparent mobility of the counterions for the polarization. The surface conductivity corresponds to the last term of equation (3) and is written as σs. A dimensionless number R has been introduced by Revil et al. (2017a) $R = \lambda / B$. From our previous studies (e.g., Ghorbani et al., 2018), we have B (Na^+, 25°C) =3.1±0.3×10^{-9} m^{2}s^{-1}V^{-1} and λ(Na^+, 25°C) =3.0±0.7×10^{-10} m^{2}s^{-1}V^{-1}, and R is typically around 0.09±0.01. In the present paper, we are interested in the dependence of the normalized chargeability with the amount of clogging matter in a horizontal subsurface flow constructed wetland filter. The CEC describes the quantity (in equivalent electrical charge) of the active (exchangeable) sites on the surface of minerals and bacteria per unit mass of minerals and/or bacteria (e.g., Revil, 2012; Revil et al., 2012). The CEC is controlled by the presence of clogging because of the increase of specific surface area caused by the clogging coating the grains (Figure 4). Therefore, the CEC can be used as a proxy of clogging weight content $\varphi_W \propto \mathrm{CEC}$ through the gravel filter.

2.2 Laboratory experiments

To test empirically the relation between normalized chargeability and the clogging content φ_W of the gravels, nine one-point induced polarization measurements were carried out on the horizontal subsurface flow constructed wetland. We use a Syscal Pro equipment (from IRIS, www.iris-instruments.com). We use 72 electrodes with a regular spacing of 0.5m and an injection time of 1 second with a dead time of 80 ms before the chargeability sampling and a total of 20 induced polarization windows (Figure 5). Then the gravel samples from the acquisition points were stored on plastic boxes to analyse them in the laboratory. On the laboratory the samples were cleaned with distilled water, this water was decanted three times and filtered to separate the clogging matter and the clean gravels. The gravel and the clogging matter from each sample were dried at 50ºC for three days and then weighed to calculate the % of clogging matter (dry) in each gravel sample.

2.3 Field data acquisition

A total of 5 induced polarization profiles (Figure 6) were acquired in the horizontal subsurface flow constructed wetland studied (Figure 1); the constructed wetland showing more evident clogging problems with surface flow of the wastewater near the inlet (Figure 7). Each one of these profiles were composed by 2 concatenated profiles with 72 stainless steel electrodes per profile in order to cover the total length of the constructed wetland without increasing the spacing between electrodes i.e. without resolution decrease. The resistivity and chargeability measurements have been carried with the Syscal Pro equipment separating the injection and acquisition electrodes to minimize the electromagnetic coupling effects as well electrode polarization issues (Dahlin and Leroux, 2012; Duvillard et al., 2018), a spacing between electrodes of 0.5 meters and 20 IP sampling windows (Figure 8). A multigradient sequence with 234 quadrupoles, an injection time of 1 second with a dead time of 80 ms before the chargeability sampling and a maximum investigation depth of 1.12 meters was selected after trial and error tests.

2.4 Inverse modelling

The filtering of the profiles has been done manually by analysing the voltage decay curves obtained in the field. We have discarded an average 19% of the decay curves in which the measurement exhibit erratic behaviours or negative voltage values. With the profiles that have already been filtered, the chargeability data (using only the first window acquired, W1) and resistivity data has been inverted with the Res2Dinv software, thus obtaining the resistivity, conductivity and chargeability of each profile, which allows finally obtaining the normalized chargeability profiles multiplying the chargeability by the conductivity cell by cell.

3. Results

3.1 Laboratory experimental results

The relationship between normalized chargeability and % clogging shows a direct correlation (R^2 = 0.76), obtaining a maximum M_n value of $10^{-2.1}$ S m^{-1} for a sample with φ_W = 4.6% clogging (dry) and a minimum value of 10^{-3} S m^{-1} for a sample with φ_W = 1.8% clogging (dry), proving that there is an increment on the normalized chargeability (more specifically on the CEC) as a consequence of an increment on the % of clogging in the filter (Figure 9). From this data we obtain the expression to calculate the % of clogging on each cell from the normalized chargeability profiles as:

$$\varphi_W(\%) = \frac{M_n}{0.0017} + 1. \quad (8)$$

3.2 Results of the induced polarization profiles and clogging estimation

The profiles made show a heterogeneous distribution of the normalized chargeability, associated with the greater or lesser presence of clogging in the gravel filter, which can be subdivided for a better compression into low (< $10^{-2.6}$ S m^{-1}), moderate (> $10^{-2.6}$ S m^{-1} < $10^{-2.2}$ S m^{-1}) and high values (> $10^{-2.2}$ S m^{-1}) (Figure 8). The electrical conductivity profiles used to calculate the M_n are presented on the Figure 11. Using the experimental formula that has been obtained (point 3.1) it is possible to obtain profiles of % clogging distribution from the M_n profiles obtained in the field, which following the criteria applied for M_n can be subdivided into low obstruction (< 2.4%), moderate obstruction (> 2.7% < 4.7%) and high obstruction (> 4.7%). The general pattern of distribution of clogging that can be inferred from the profiles herein presented shows an upper layer with low obstruction, except at the profile start (water inlet) that has moderate obstruction values, that passes to moderate and high obstruction values in depth (Figure 10).

We also present 5 depth slices of the constructed wetland for M_n (Figure 12) and percent of clogging (Figure 13) with depths at -0.1 m, -0.32 m, -0.56 m, -0.83 m and -1.12 m. To simplify compression only percent of clogging profiles are described since they are the final objective of the present study.

In the -0.1m and -0.32 m slices the percent of clogging are similar, with low percent of clogging values in the middle part of the constructed wetland and moderate values at the start (water inlet) and on a zone at the end (water outlet). The -0.56m slice shows moderate obstruction values except in its central part following the flow direction were low obstruction values are shown. This trend is also observed in the -0.83m slice were high obstruction values are dominant in the laterals and at the end of the constructed wetland, but moderate obstruction values are located at the start and at the central part of the constructed wetland. The -1.12 m slice shows, in general, smaller obturation values than the -0.83 m slice, with the higher obturation values still on the laterals of the constructed wetland but occupying a smaller area being the moderate obstruction values dominant.

4. Discussion

The technique herein presented allows to anticipate the critical situation involved in the clogging of the filter since it is able to detect the areas where clogging is concentrated in a fast, economical, effective way and easily replicable in time, thus giving information on the evolution of this clogging and without need to stop the normal operation of the plant. Normalized chargeability depends on the cation exchange capacity (CEC), which will be increased in areas where clogging is accumulating thanks to the fixation of clay particles and to the increase of the specific surface area caused by this clogging coating the gravel. The depth slices give valuable information about the areas where clogging is accumulating and an estimate of the accumulated amount; the two most superficial slices (-0.1 m and -0.32 m) show that in general the condition of the filter at these depths is good except for a part of the final zone (water outlet) and the start zone (water inlet) that shows some higher clogging values, corroborated in the field since it is in these first meters of the filter that surface water flow is observed. The slice corresponding to a depth of 0.56 m shows moderate clogging values except in the central part of the filter, where they are low.

In this distribution, two problems are obvious. The degree of clogging increases with depth clogging is not homogeneously distributed, which generates preferential water flow paths. The highest clogging values are shown at a depth of 0.83 m, on the sides of the filter giving rise to a preferred water flow zone at the beginning and through the center of the filter. The deepest slice corresponds to a depth of 1.12 m where differences in the degrees of clogging are also observed, which continues to give rise to preferential flow zones. These data show the existence of differences in the degree of clogging of the filter that in general is greater in depth, but if we observe in detail the depth slices we can identify for the same depth areas with greater and lesser degree of clogging and therefore areas of preferential flow and areas with a more residual flow or even without flow which will favour the formation of more clogging and drastically reducing the effectiveness of the system. The information obtained with the method presented here allows to identify the areas where clogging is being concentrated. This could offer the possibility to monitor the occurrence of clogging over time, which can be useful to anticipate potential problems such as surface water flow or the creation of areas without flow in depth. It is possible to plan a partial substitution of the gravels, affecting only the area of high clogging values, thus reducing both the economic cost of the operation and the time to stop the system.

5. Conclusions

Time-domain induced polarization is used for the first time to image clogging distribution of a gravel filter from a horizontal subsurface flow constructed wetland.

Experimental data performed on the laboratory demonstrates the linear relationship between the normalized chargeability and the amount of clogging in the gravel filter because of the substantial increase of the cation exchange capacity caused by clogging coating these grains. This is expected since clogging contains fine particles and bacteria characterized by high cation exchange capacity. Therefore, we were able to convert the 3D normalized chargeability tomogram obtained with the field data into a 3D distribution of the percent clogging. This method allows to identify the zones were the clogging has accumulated trough the filter and therefore predict preferential flow paths and dead flow zones. This is an important task to plan preventive measures and anticipate the filter obstruction that may decreases the effectiveness of the waste water treatment system.

Acknowledgements

This work is supported by Water Research Institute (IdRA) from the University of Barcelona and by the predoctoral grant APIF from the University of Barcelona. We also thank the help and the support provided in the field by both Angel Lázaro and Montse Palomes from Aigües de Catalunya.

References

Archie, G.E., 1942. The electrical resistivity log as an aid in determining some reservoir characteristics. Transactions of the AIME. Society of Petroleum Engineers, 146, 54-62. https://doi.org/10.2118/942054-G

Dahlin, T., Leroux, V., 2012. Improvement in time-domain induced polarization data quality with multi-electrode systems by separating current and potential cables. Near Surface Geophysics, 10, 545-565. https://doi.org/10.3997/1873-0604.2012028

Duvillard P.A., Revil, A., Soueid Ahmed, A., Qi, Y., Coperey, A., Ravanel, L., 2018. Three-dimensional electrical conductivity and induced polarization tomography of a rock glacier, Journal of Geophysical Research, 123, 9528-9554. https://doi.org/10.1029/2018JB015965

Licciardello, F., Aiello, R., Alagna, V., Iovino, M., Ventura, D., Cirelli, G.L. 2019. Assessment of clogging in constructed wetlands by saturated hydraulic conductivity measurements. Water Science & Technology, 79, 314-332. https://doi.org/10.2166/wst.2019.045

Marzo, A., Ventura, D., Cirelli, G.L., Aiello, R., Vanella, D., Rapisarda, R., Barbagallo, S., Consoli, S., 2018. Hydraulic reliability of a horizontal wetland for wastewater treatment in Sicily. Science of the Total Environment, 636, 94-106. https://doi.org/10.1016/j.scitotenv.2018.04.228

Matos, M.P., von Sperling, M., Matos, A.T., Aranha, P.R.A., Santos, M.A., Pessoa, F.D.B., Viola, P.D.D. 2019. Clogging in constructed wetlands: Indirect estimation of medium porosity by analysis of ground-penetrating radar images. Science of the

Total Environment, 676, 333-342. https://doi.org/10.1016/j.scitotenv.2019.04.168

Nivala, J., Rousseau, D.P.L., 2009. Reversing clogging in subsurface-flow constructed wetlands by hydrogen peroxide treatment: two case studies. Water Science & Technology, 59, 2037-2046. https://doi.org/10.2166/wst.2009.115

Pedescoll, A., Corzo, A., Álvarez, E., García, J., Puigagut, J., 2011. The effect of primary treatment and flow regime on clogging development in horizontal subsurface flow constructed wetlands: An experimental evaluation. Water Research, 45, 3579-3589. https://doi.org/10.1016/j.watres.2011.03.049

Puigagut, J., Villaseñor, J., Salas, J.J., Bécares, E., García, J., 2007. Subsurface-flow constructed wetlands in Spain for the sanitation of small communities: a comparative study. Ecological Engineering, 30 (4), 312-319. https://doi.org/10.1016/j.ecoleng.2007.04.005

Revil, A., Florsch, N., 2010. Determination of permeability from spectral induced polarization data in granular media, Geophysical Journal International, 181, 1480-1498. https://doi.org/10.1111/j.1365-246X.2010.04573.x

Revil, A., 2012. Spectral induced polarization of shaly sands: Influence of the electrical double layer, Water Resour. Res., 48, W02517. https://doi.org/10.1029/2011WR011260

Revil, A., Atekwana, E., Zhang, C., Jardani, A., Smith, S., 2012. A new model for the spectral induced polarization signature of bacterial growth in porous media, Water Resour. Res., 48, W09545. https://doi.org/10.1029/2012WR011965

Revil, A, 2013a. Effective conductivity and permittivity of unsaturated porous materials in the frequency range 1 mHz–1GHz. Water Resources Research 49, 306–327.

https://doi.org/10.1029/2012WR012700

Revil, A., 2013b. On charge accumulations in heterogeneous porous materials under the influence of an electrical field. Geophysics 78 (4), D271–D291. https://doi.org/10.1190/geo2012-0503.1

Revil, A., Ahmed, A. Soueid, Jardani, A., 2017a. Self-potential: a non-intrusive ground water flow sensor. J. Environ. Eng. Geophys. 22 (3), 235–247. https://doi.org/10.2113/JEEG22.3.235

Revil, A., Coperey, A., Shao, Z., Florsch, N., Fabricius, I.L., Deng, Y., Delsman, J.R., Pauw, P.S., Karaoulis, M., de Louw, P.G.B., van Baaren, E.S., Dabekaussen, W., Menkovic, A., Gunnink, J.L., 2017b. Complex conductivity of soils. Water Resour. Res. 53, 7121-7147. https://doi.org/10.1002/2017WR020655

Rosen, L., Baygents, J., Saville, D., 1993. The interpretation of dielectric response measurements on colloidal dispersions using the dynamic Stern layer model. The Journal of chemical physics 98, 4183–4194. https://doi.org/10.1063/1.465108

Schlumberger, C., 1920. Study of underground electrical prospecting. 99 pp. Paris.

Seigel, H.O., 1959. Mathematical formulation and type curves for induced polarization. Geophysics 24, 547–565. https://doi.org/10.1190/1.1438625

Tapias, J.C., Himi, M., Lovera, R., Folch, M., Font, X., Casas, A., 2013. Evaluación mediante tomografia de resistividad eléctrica de las propiedades hidráulicas de la zona saturada y no-saturada de humedales artificiales para el tratamiento de agua residual. Estudios de la Zona no Saturada del Suelo, 11, 51-55.

Vera, I., García, J., Sáez, K., Moragas, L., Vidal, G., 2011. Performance evaluation of eight years experience of constructed wetland systems in Catalonia as alternative treatment for small communities. Ecological Engineering, 37, 364-371. https://doi.org/10.1016/j.ecoleng.2010.11.031

Vinegar, H.J., Waxman, M.H., 1984. Induced Polarization of Shaly Sands. Geophysics, 49, 1267-1287. http://dx.doi.org/10.1190/1.1441755

Vymazal, J., 2005. Horizontal sub-surface flow and hybrid constructed wetlands systems for wastewater treatment. Ecological Engineering, 25, 478-490.

Vymazal, J., 2011. Constructed wetlands for wastewater treatment: five decades of experience. Environmental Science & Technology, 45, 61-69. https://doi.org/10.1016/j.ecoleng.2005.07.010

Zhang, C., Revil, A., Fujita, Y., Munakata-Marr, J., Redden, G., 2014. Quadrature conductivity: a quantitative indicator of bacteria abundance in porous media, Geophysics, 79(6), D363–D375. https://doi.org/10.1190/GEO2014-0107.1

Figures

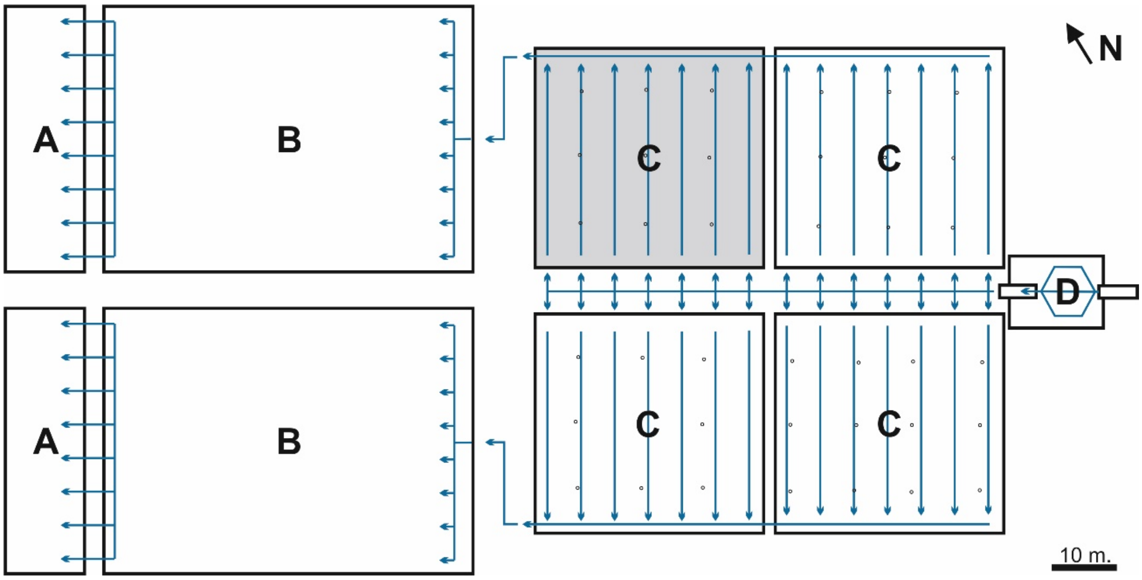

Figure 1. Verdú horizontal subsurface flow constructed wetland scheme. A; small horizontal subsurface flow constructed wetlands, B; maturation ponds, C; horizontal subsurface flow constructed wetlands and D; pre-treatment stage. The arrows indicate the flow direction. The horizontal subsurface flow constructed wetland shaded in grey in the studied filter.

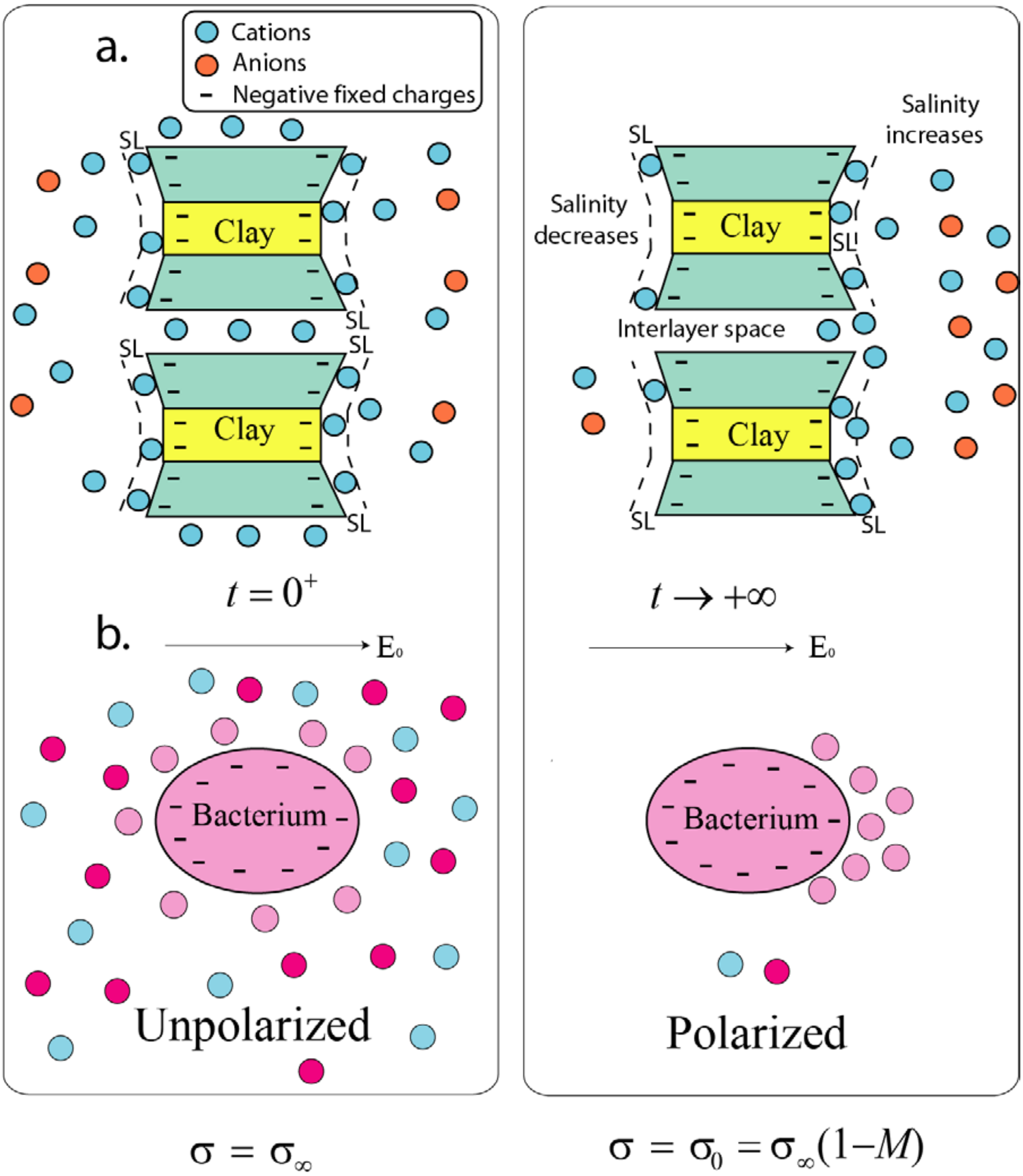

Figure 2. Clogging can be made of fine particles and biofilms formed by bacteria, **a.** In an imposed electrical field $\mathbf{E}_0$, Fine particles like here a clay particle get polarized. **b.** In a similar way, bacteria gets polarized in an applied electrical field. In both cases, the polarized particle behaves like a dipole generating a secondary electrical field, responsible for the observed induced polarization. The short application of the electrical field defines the instantaneous conductivity while a long application of the electrical field defines the Direct Current (DC) conductivity.

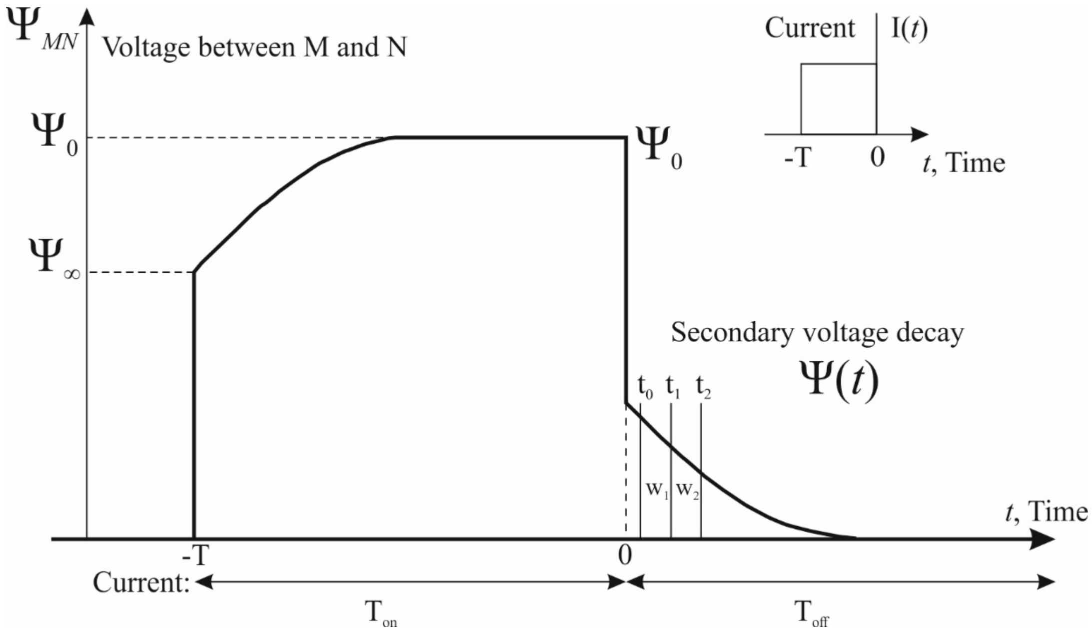

Figure 3. Time-domain induced polarization measurements. Measured potential difference between two voltage electrodes M and N for a box current input through current electrodes A and B. The decaying secondary voltage (for $t > 0$) is sampled into windows (W_1, W_2, etc.) separated by characteristic times (t_0, t_1, t_2, …). The partial or apparent chargeabilities are determined for each of these windows by integrating the voltage decay over the duration of the window.

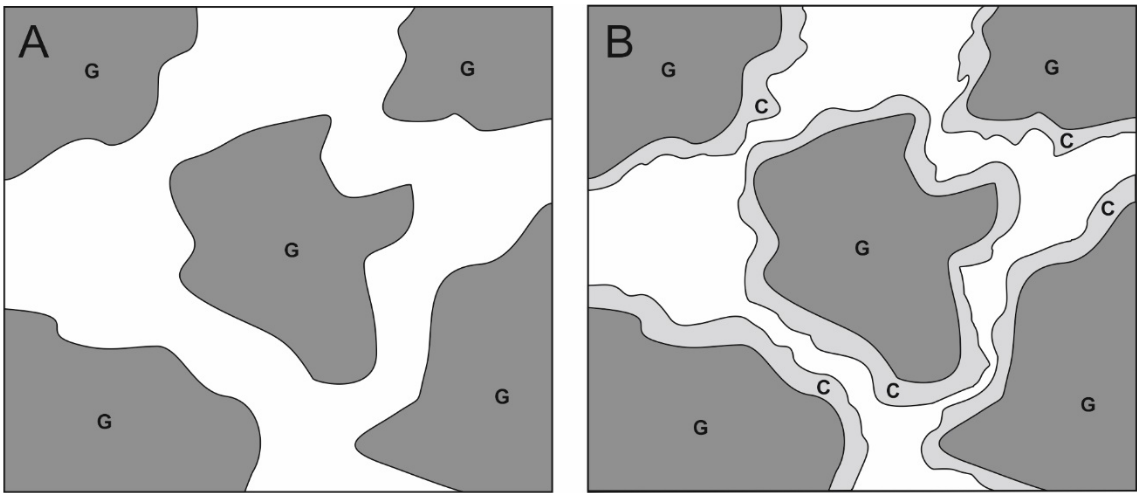

Figure 4. Influence of clogging on the texture. A) Microscopic scheme without clogging. B) Microscopic scheme with clogging coating the grains, showing how this clogging may block the water flow and how the specific surface area able to exchange cations is increased (i.e. how the CEC is increased and therefore the normalized chargeability). G = gravel grains, C = Clogging.

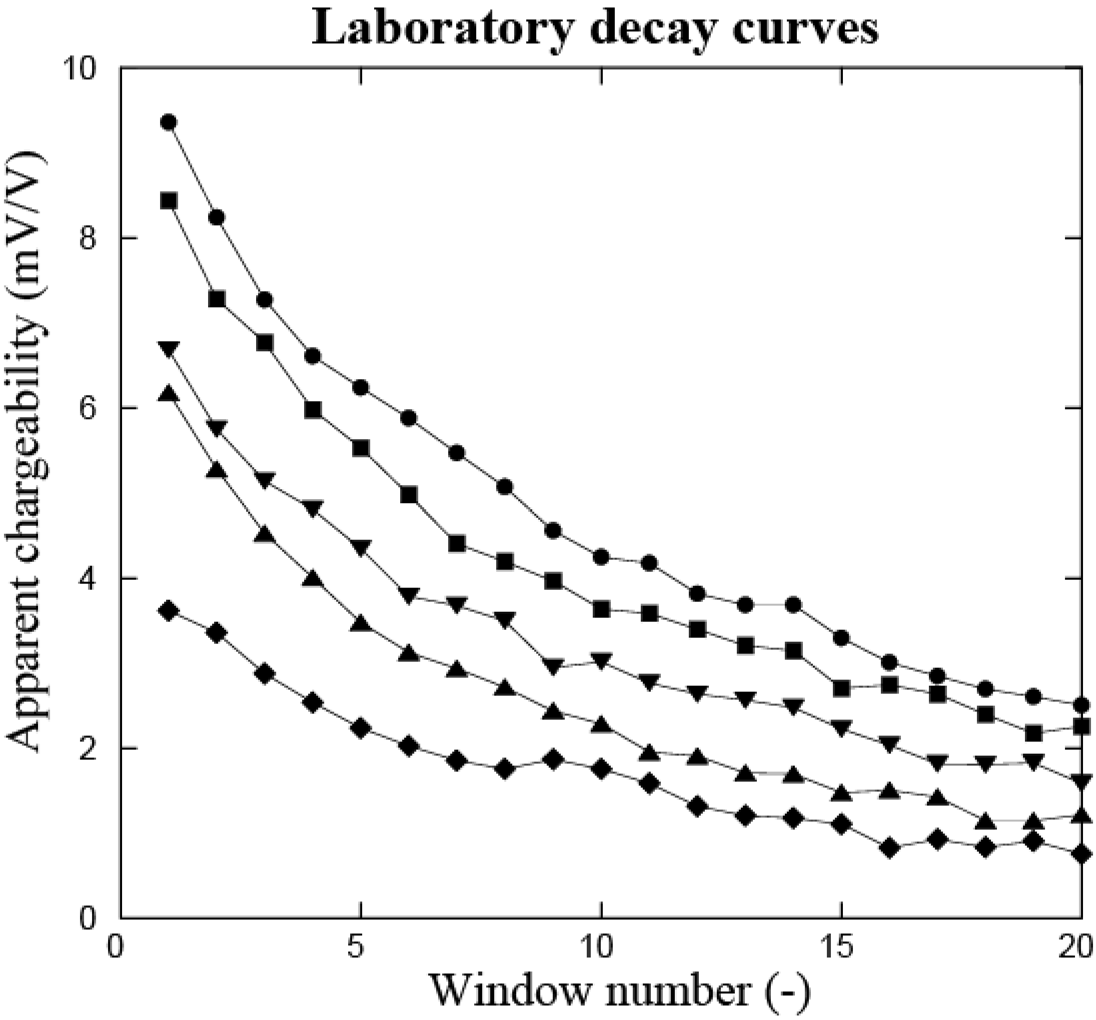

Figure 5. Apparent chargeability decay curves for 5 of the samples used in the laboratory to test the correlation between the normalized chargeability and the percent of clogging. We have sampled the voltage decay over 20 windows W_i (i from 1 to 20). The lines are just guides for the eyes.

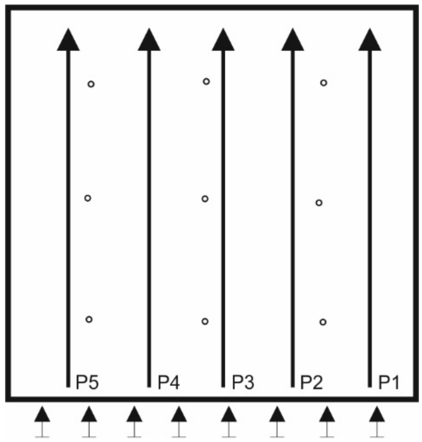

Figure 6. Location of the five induced polarization profiles (P1 to P5) on the horizontal subsurface flow constructed wetland studied. The small arrows indicate the water inlet and the flow direction from the inlet inward.

Figure 7. Picture of the constructed wetland investigated in the present paper. The surface flow can be seen along the water inlet as well as the nine piezometers.

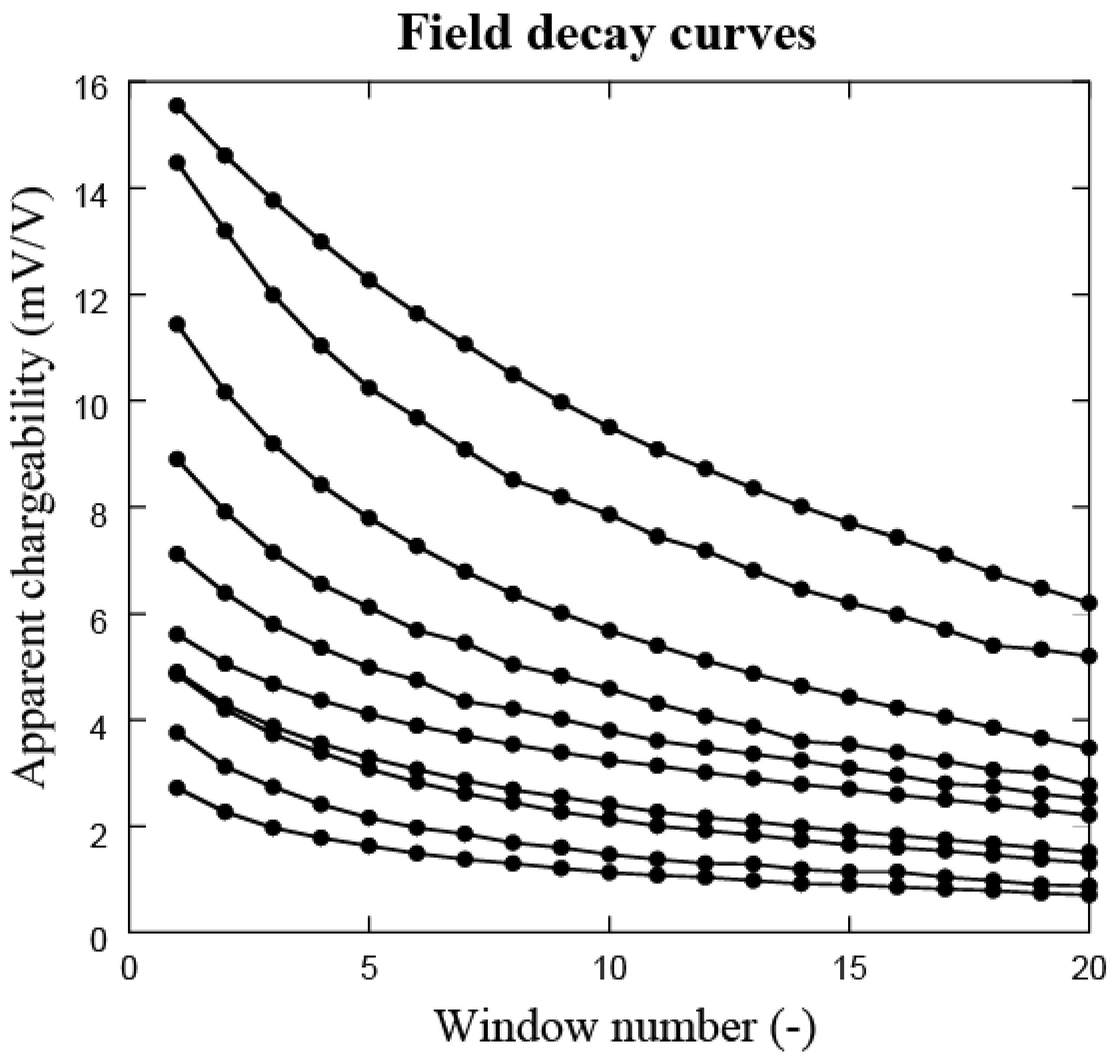

Figure 8. Selected apparent chargeability decay curves from the field profiles. We have sample the voltage decay over 20 windows like for the laboratory data. The range of the apparent normalized chargeability is reasonably similar in the field and in the laboratory. The lines are just guides for the eyes.

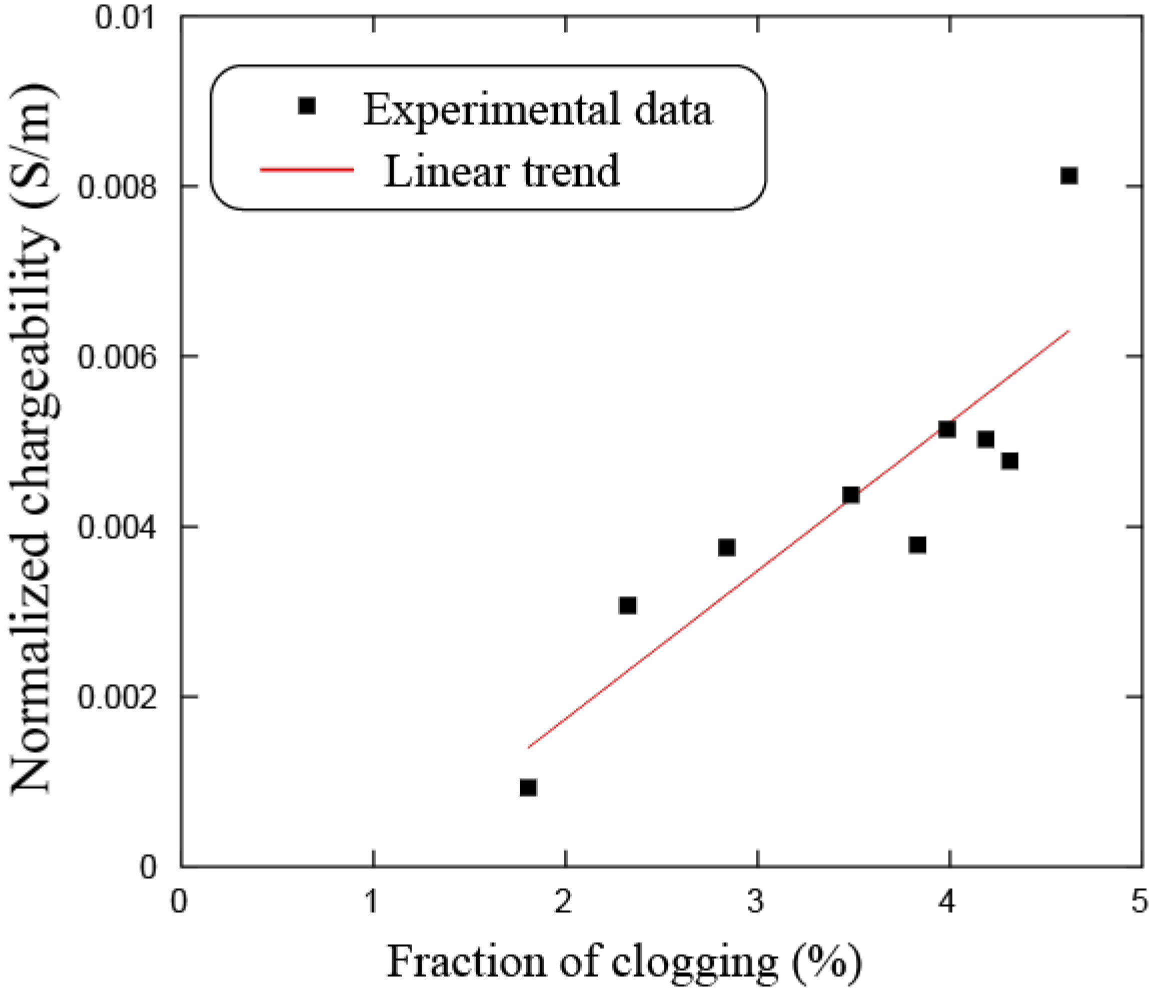

Figure 9. Normalized chargeability versus percent of clogging graphic from the laboratory samples. The correlation coefficient is R = 0.873.

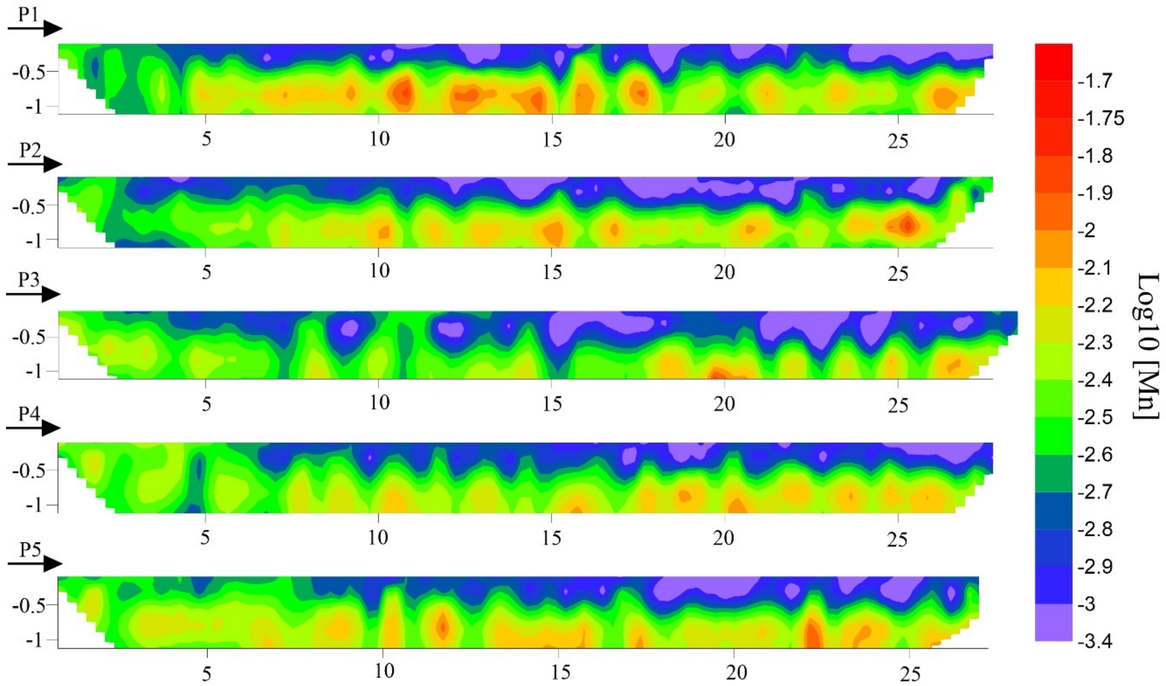

Figure 10. Normalized chargeability profiles (P1-P5) inverted. The black arrow indicates the water inlet and the flow direction, SW-NE.

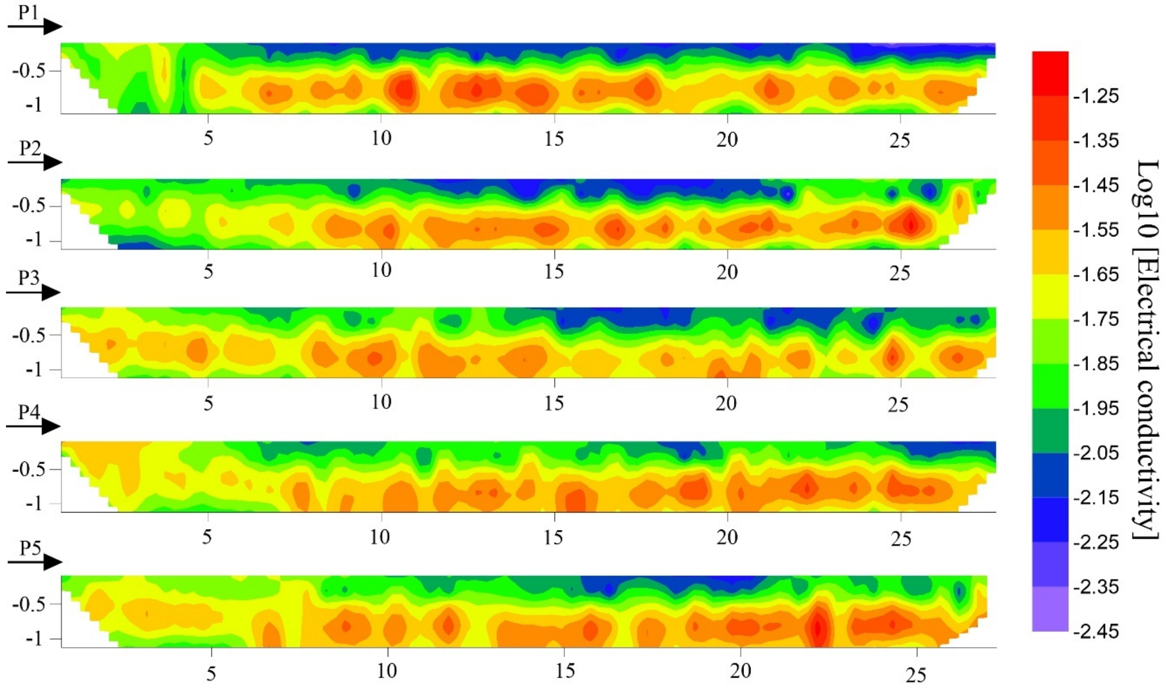

Figure 11. Conductivity profiles (P1-P5) inverted. The black arrow indicates the water inlet and the flow direction, SW-NE.

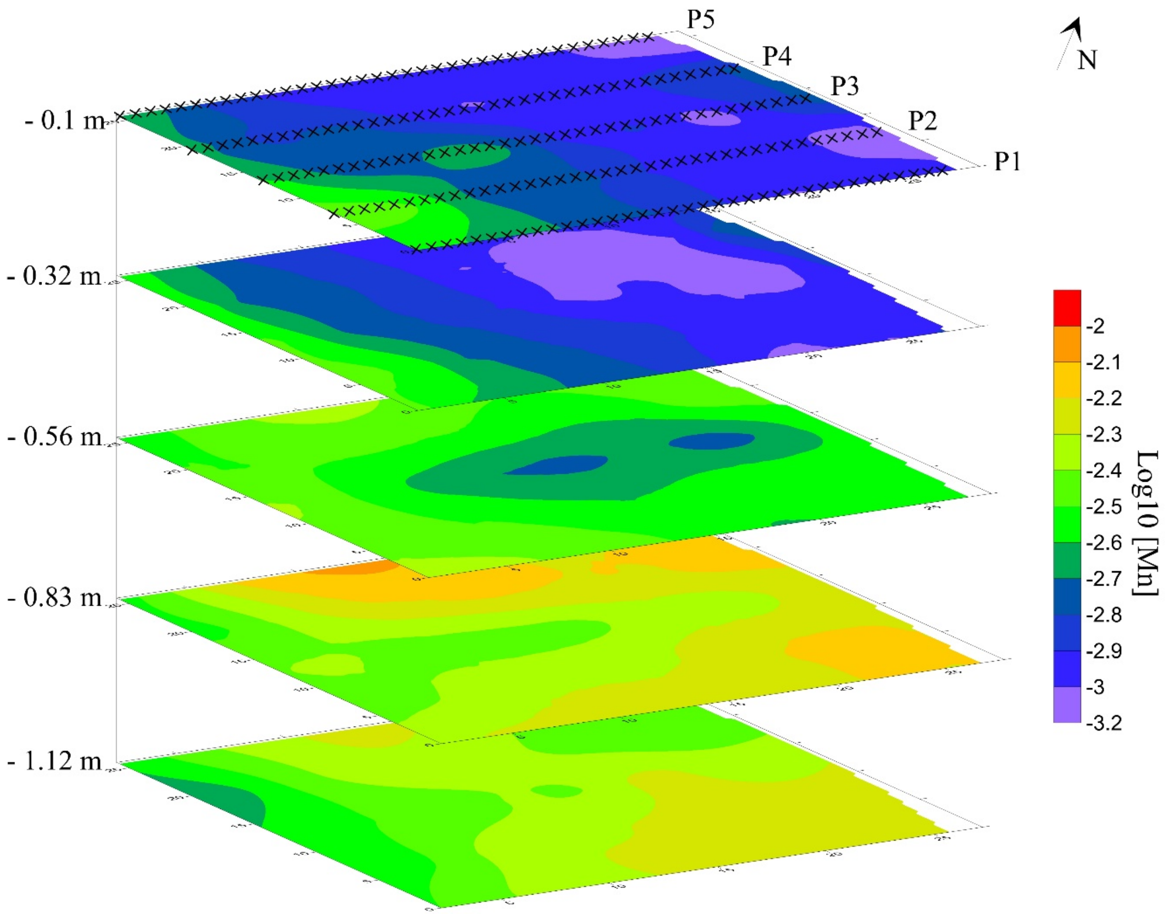

Figure 12. Normalized chargeability (in S/m) depth slices. The crosses show the electrode locations at the ground surface.

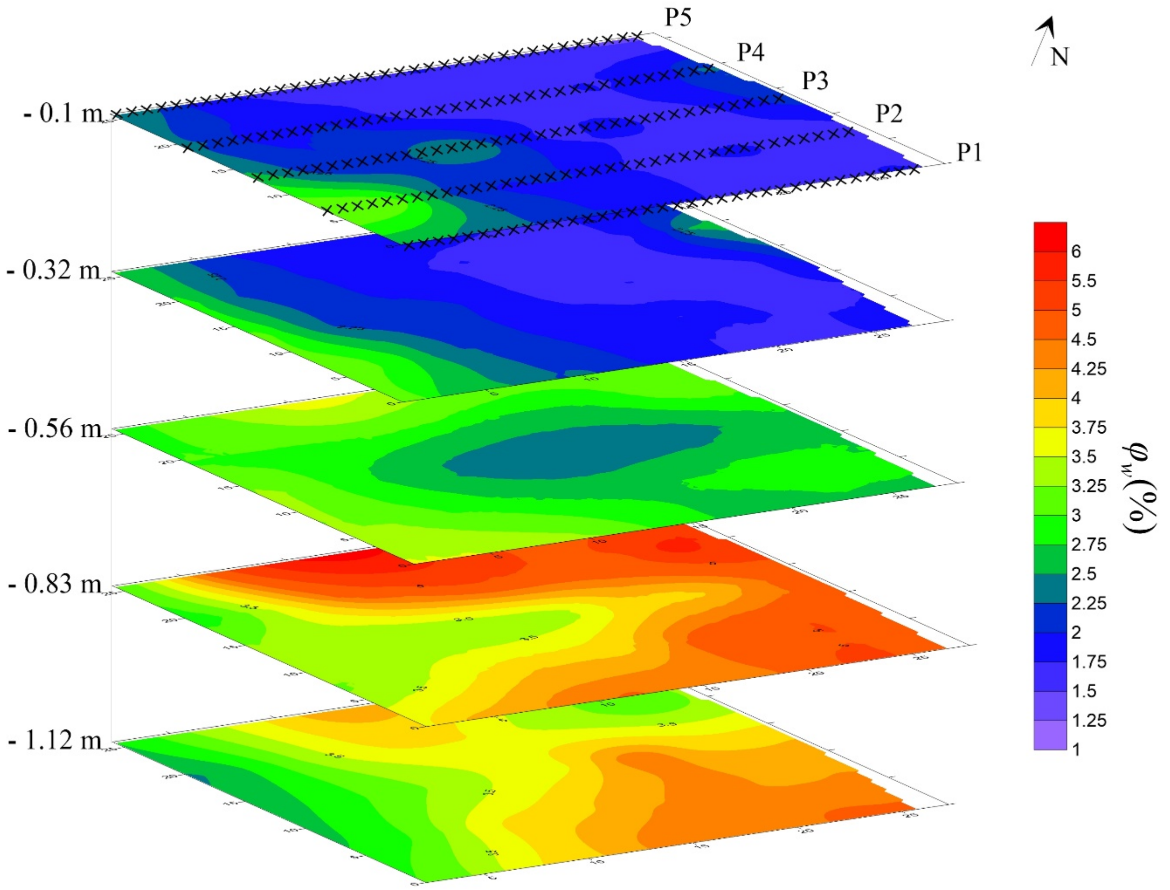

Figure 13. Percent of clogging depth slices obtained with the expression presented on the point 3.1. The crosses denote the electrode locations at the ground surface.